

図1：QM/MM計算により得られたRT-阻害剤（thujaplicinol）複合体構造
 昨年度まで構築した構造全体を動かしてエネルギー極小化した構造（緑）と今年度行ったQM部分だけを動かした構造（青）を示す。後者の方が、実験構造に類似しており適切な構造モデルだと考えられる。

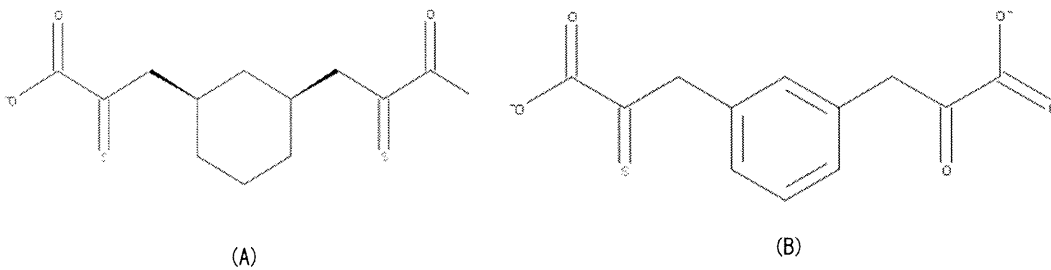


図2：昨年度まで計算により検出されたヒット薬剤

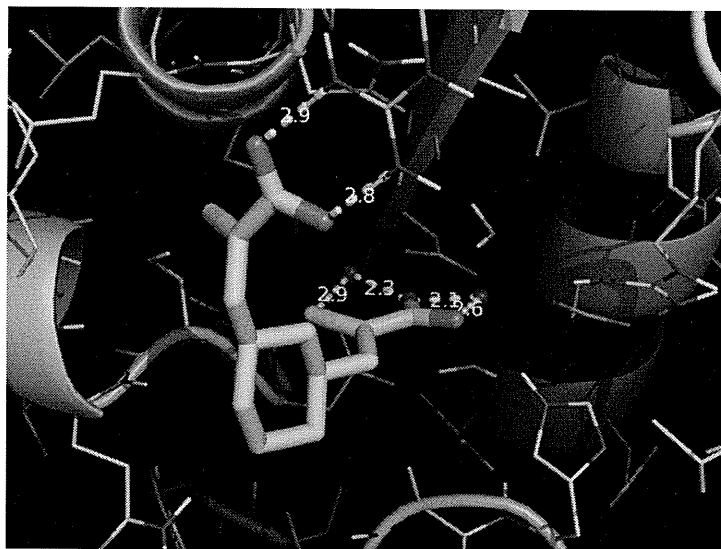


図3：QM/MM計算により得られたRT-阻害剤（図2）複合体構造。

薬剤(図2(A))は、2つの官能基(sulfanylidenepranoic acid)の一方をRNase Hドメインの活性中心にある2つのMg²⁺へ配位させ、もう一方の官能基はタンパク質表面に存在するアルギニンと水素結合を形成している結合様式が最安定なポテンシャルエネルギーを示した。

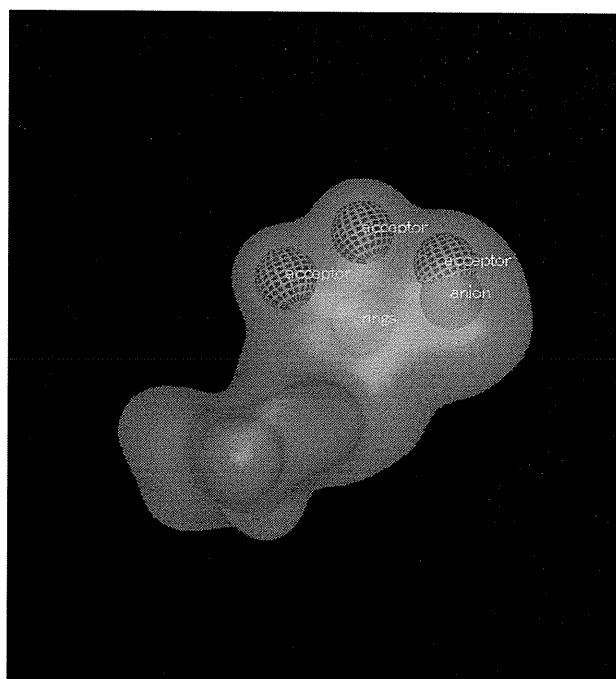


図4：薬剤探索に使用した分子形状クエリー

数種の既知薬剤構造から体積の重なりを考慮した分子体積モデルを構築し、更に、この体積モデル上に水素結合ドナーやアクセプターなどのファーマコフォア情報を付加した分子形状クエリーを構築した。この分子形状クエリーを用いて、薬剤探索を行った。

研究成果の刊行に関する一覧表

雑誌

発表者氏名	論文タイトル	発表誌名	巻号	ページ	出版年
Yanagita H., Fudo S., Urano E., Ichikawa R., Ogata M., Yokota M., <u>Murakami T.</u> , Wu H., Chiba J., <u>Komano J.</u> , <u>Hoshino T.</u>	Structural Modulation Study of Inhibitory Compounds for RNase H Activity of HIV-1 Reverse Transcriptase	Chem. Pharm. Bull.	60 (6)	in press	2012
Yanagita H., Yamamoto N., Fuji H., Liu X., Ogata M., Yokota M., Takaku H., Hasegawa H., Odagiri T., Tashiro M., <u>Hoshino T.</u>	Mechanism of drug resistance of hemagglutinin of influenza virus and potent scaffolds inhibiting its function	ACS Chem. Biol.	7 (3)	552-562	2012
Takizawa M., Miyauchi K., Urano E., Kusagawa S., Kitamura K., Naganawa S., Murakami T., Honda M., Yamamoto N., <u>Komano J.</u>	Regulation of the susceptibility of HIV-1 to a neutralizing antibody KD-247 by non-epitope mutations distant from its epitope	AIDS.	in press	in press	2012
Nomura W., Hashimoto C., Ohya A., Miyauchi K., Urano E., Tanaka T., Narumi T., Nakahara T., <u>Komano J.</u> , Yamamoto N., Tamamura H.	Synthetic C34 Trimer of HIV-1 gp41 Shows Significant Increase of Inhibition Potency	Chem. Med. Chem.	in press	in press	2012
Watanabe T., Urano E., Miyauchi K., Ichikawa R., Hamatake M., Misawa N., Sato K., Ebina H., Koyanagi Y., <u>Komano J.</u>	The hematopoietic cell-specific Rho GTPase inhibitor ARHGDIB/D4GDI limits HIV-1 replication	AIDS Res. Hum. Retrovirus es.	in press	in press	2012
Imadome K., Yajima M., Arai A., Nakagawa-Nakagawa A., Kawano F., Ichikawa S., Shimizu N., Yamamoto N., Morio T., Ohga S., Nakamura H., Ito M., Miura O., <u>Komano J.</u> , Fujiwara S.	CD4-positive T cells have a critical role in the proliferation of EBV-infected T and NK cells	PLOS Pathog.	in press	in press	2012
Urano E., Kuramochi N., Tomoda H., Takebe Y., Miyauchi K., <u>Komano J.</u> , Morikawa Y.	A Novel Postentry Inhibitor of Human Immunodeficiency Virus Type 1 Replication Screened by Yeast Membrane-associated Two-hybrid System	Antimicrob. Agents Chemother.	55 (9)	4251-60	2011
Aoki T., Miyauchi K., Urano E., Ichikawa R., <u>Komano J.</u>	Protein transduction by pseudotyped lentivirus-like nanoparticles	Gene Ther.	18 (9)	936-41	2011

Li J., Hakata Y., Takeda E., Liu Q., <u>Iwatani Y.</u> , Kozak CA., Miyazawa M.	Two genetic determinants acquired late in Mus evolution regulate the inclusion of exon5, which alters mouse APOBEC3 translation efficiency	PLoS Pathogens	8	E1002478	2012
Kitamura S., Ode H., <u>Iwatani Y.</u>	Structural features of antiviral APOBEC3 proteins are linked to their functional activities	Frontiers in Microbiol.	2	258	2011
Shibata J., Sugiura W., Ode H., <u>Iwatani Y.</u> , Sato H., Tsang H., Matsuda M., Hasegawa N., Ren F., Tanaka H.	Within-host co-evolution of Gag P453L and protease D30N/N88D demonstrates virological advantage in a highly protease inhibitor-exposed HIV-1 case	Antiviral Res.	90	33-41	2011
Narumi T., Komoriya M., Hashimoto C., Wu H., Nomura W., Suzuki S., Tanaka T., Chiba J., Yamamoto N., <u>Murakami T.</u> , Tamamura H.	Conjugation of cell-penetrating peptides leads to identification of anti-HIV peptides from matrix proteins.	Bioorg. Med. Chem.	20	1468-1474	2012
Tanaka T., Narumi T., Ozaki T., Sohma A., Ohashi N., Hashimoto C., Itotani K., Nomura W., <u>Murakami T.</u> , Yamamoto N., Tamamura H.	Azamacrocyclic-metal complexes as CXCR4 antagonists. Azamacrocyclic-metal complexes as CXCR4 antagonists.	Chem. Med. Chem.	6	834-839	2011
Taiji M., <u>Okimoto N.</u>	高性能計算による薬剤分子設計	日本化学会情報化学部会誌	29	55-60	2011
Kondo H., <u>Okimoto N.</u> , Morimoto G., Taiji M.	Free-Energy Landscapes of Protein Domain Movements upon Ligand Binding	J. Phys. Chem. B	115	7629-7636	2011

Structural Modulation Study of Inhibitory Compounds for Ribonuclease H Activity of Human Immunodeficiency Virus Type 1 Reverse Transcriptase

Hiroshi Yanagita,^a Satoshi Fudo,^a Emiko Urano,^b Reiko Ichikawa,^b Masakazu Ogata,^a Mizuho Yokota,^a Tsutomu Murakami,^b Honggui Wu,^{b,c} Joe Chiba,^c Jun Komano,^b and Tyuji Hoshino^{*a}

^a Graduate School of Pharmaceutical Sciences, Chiba University; 1–8–1 Inohana, Chuo-ku, Chiba 260–8675, Japan; ^b AIDS Research Center, National Institute of Infectious Diseases; 1–23–1 Toyama, Shinjuku-ku, Tokyo 162–8640, Japan; and ^c Faculty of Industrial Science and Technology, Tokyo University of Science; 2641 Yamazaki, Noda, Chiba 278–8510, Japan. Received February 23, 2012; accepted April 4, 2012

Reverse transcriptase of human immunodeficiency virus type 1 (HIV-1) has two enzymatic functions. One of the functions is ribonuclease (RNase) H activity concerning the digestion of only RNA of RNA/DNA hybrid. The RNase H activity is an attractive target for a new class of anti-HIV drugs because no approved inhibitor is available now. In our previous studies, an agent bearing 5-nitro-furan-2-carboxylic acid ester core was found from chemical screening and dozens of the derivatives were synthesized to improve compound potency. In this work, some parts of the chemical structure were modulated to deepen our understanding of the structure–activity relationship of the analogous compounds. Several derivatives having nitro-furan-phenyl-ester skeleton were shown to be potent RNase H inhibitors. Attaching methoxy-carbonyl and methoxy groups to the phenyl ring increased the inhibitory potency. No significant cytotoxicity was observed for these active derivatives. In contrast, the derivatives having nitro-furan-benzyl-ester skeleton showed modest inhibitory activities regardless of attaching diverse kinds of functional groups to the benzyl ring. Both the modulation of the 5-nitro-furan-2-carboxylic moiety and the conversion of the ester linkage resulted in a drastic decrease in inhibitory potency. These findings are informative for designing potent inhibitors of RNase H enzymatic activity of HIV-1.

Key words antiviral drug; human immunodeficiency virus type 1 reverse transcriptase; ribonuclease H enzymatic activity; inhibitor; nitro-furan-phenyl-ester

Human immunodeficiency virus type 1 (HIV-1) reverse transcriptase (RT) is a multi-functional enzyme that facilitates both polymerase and ribonuclease (RNase) H activities and converts the single-stranded viral RNA into a double-stranded DNA. There exist two active sites in HIV-1 RT responsible for the respective enzymatic functions. Currently, two classes of RT inhibitors, nucleoside reverse transcriptase inhibitors (NRTIs) and non-nucleoside reverse transcriptase inhibitors (NNRTIs), are used clinically. The formers compete with the natural deoxyribonucleotide triphosphate (dNTP) for nucleoside incorporation and act as chain terminators after incorporation.¹⁾ The latter agents are bound to an adjacent location from the polymerase active site and block RT polymerase function.²⁾ Both of these inhibitors are targeting polymerase activity of RT. In contrast, no approved inhibitor is available for RNase H activity, although there have been several reports on the inhibitors that target the RNase H activity of HIV-1 RT.^{3–5)} The role of RNase H activity in the reverse transcription process is to remove the viral genomic RNA during the synthesis of double-stranded DNA.^{6,7)} Agents targeting RNase H function is expected to be complimentary to the currently standard chemotherapy. Hence, RT-associated RNase H activity is one of the attractive targets for developing a novel class of antiviral drugs. Furthermore, the potential for dual inhibition of RNase H activity and integrase activity of HIV-1 has been examined because of the structural similarity of their catalytic sites.^{8–10)}

HIV-1 RNase H is known to utilize two divalent metals for

catalysis.^{11–13)} The RNase H dual metal mechanism was suggested from high resolution co-crystal structures of *B. halodurans* RNase H with RNA/DNA hybrids at different stages along the reaction pathway of phosphodiester cleavage.^{14,15)} The active site contains four carboxyl residues, creating an environment capable of holding two metal ions. It has been assumed that many RNase H inhibitors bind to the catalytic center interacting with two divalent metal ions simultaneously.

Diketo acids are known to work as potent inhibitors for divalent metal-related enzymes.¹⁶⁾ Therefore, diketo acid structure has served as a starting point for the design and optimization of inhibitors of HIV-1 integrase or influenza endonuclease. Pyrimidinol is another typical agent bearing a scaffold called *N*-hydroxyimide.¹⁷⁾ *N*-Hydroxyimides were firstly described as inhibitors of influenza endonuclease, but they also show a high potency in biochemical assays of HIV-1 RNase H. A natural product β -thujaplicinol is another scaffold and shows a high inhibitory potency for HIV-1 RNase H activity.¹⁸⁾

From an *in vitro* screening using 20000 chemical compounds, we found chemicals that blocked HIV-1 RT-associated RNase H activity.¹⁹⁾ The agents bearing the 5-nitro-furan-2-carboxylic acid ester moiety turned out to work as an RNase H inhibitor. Two of the agents were capable of suppressing HIV-1 replication in tissue culture. On the basis of the hit chemicals found in the screening, more than 50 derivatives of 5-nitro-furan-2-carboxylic acid were synthesized.²⁰⁾ Inhibitory potency of RNase H enzymatic activity was measured in a biochemical assay. Several derivatives showed higher inhibitory activities than those of the hit chemicals. Modulation of

The authors declare no conflict of interest.

* To whom correspondence should be addressed. e-mail: hoshino@chiba-u.jp

the 5-nitro-furan-2-carboxylic moiety resulted in a decrease in inhibitory potency. In contrast, many derivatives with modulation of other parts maintained inhibitory activities. These studies indicate that the nitro-furan-carboxylic moiety is one of the potent scaffolds for RNase H inhibitor.

In this study, we further synthesized chemical compounds bearing the 5-nitro-furan-2-carboxylic acid ester moiety and examined the potency for anti-HIV drugs blocking RT-associated RNase H enzymatic activity. The potency of the synthesized compounds was evaluated through the measurement of inhibitory activity with real-time monitoring of fluorescence emission from the digested RNA substrate. In addition, the cytotoxicity of these compounds was assessed in 293T cells. Computer simulation with molecular dynamics (MD) method was also performed to analyze the stability of the binding structure of an active compound.

Experimental

Organic Synthesis Compound **1** was synthesized by creating an ester linkage between a nitro-furan carboxylic acid and an α -chloro-amide bound with benzyl and pentyl groups, by 3 h reaction at 60°C in dimethylformamide (DMF) in the presence of dimethyl-aminopyridine (DMAP). Chemical modulation was performed for the nitro-furan moiety, with changing the starting block from furan to thiophene or pyrrole *etc.* **2–8**. These compounds **2–8** were synthesized in the similar manner to compound **1**. The derivatives bearing 5-nitro-furan-2-ester scaffold, compounds **9–27**, were prepared by the reaction of converting 5-nitro-2-furoic acid into an acid chloride with thionyl chloride, followed by the nucleophilic substitution reaction in the presence of NEt₃ in tetrahydrofuran (THF) with setting the temperature at 0°C for the initial 30 min. and elevated it to r.t. afterward. Since a hydroxy group bound to phenyl ring is more reactive than a hydroxy group bound to alkane, the substitution reaction dominantly produced phenyl-ester linkage (**9–16**) when a nucleophilic reagent contained two hydroxy groups. When a nucleophilic reagent contained only one hydroxy group, the substitution reaction generated alkyl-ester linkage (**17–27**). Compounds **28–30** were produced by generating nitro-furan-carbonyl-alkyl-benzene through the reaction of Weinreb amides containing benzyl group with alkyl lithium, followed by incorporation of nitro group into the phenyl ring using white fuming nitric acid and acetic anhydride. Compounds **29** and **30** were separated by flash chromatography. Compounds **31–33** were generated by using hydroxy-amines as nucleophilic reagents.

Evaluation of Inhibitory Activity The 50% inhibitory concentration (IC₅₀) of the synthesized compounds for RT-associated RNase H activity was determined from the chemical concentration reducing the rate for substrate cleavage reaction to half relative to the control. A real-time monitoring assay was employed to estimate the IC₅₀.^{21,23} In short, two oligo-nucleotides were annealed at final concentrations of 2.5 and 0.25 μ M for substrate. One was oligo-ribonucleotide 5'-GAUCUGAGCCUGGGAGCU-3' with 6-carboxy-fluorescein (FAM) conjugated at the 3' end, and the other was oligo-deoxyribonucleotide 5'-AGCTCCCAGGCTCAGATC-3' with black hole quencher (BHQ) conjugated at the 5' end. Enzyme reaction with 100 ng RT, 0.025 μ M oligo-ribonucleotide, and 0.25 μ M oligo-deoxyribonucleotide was carried out in a volume of 10 μ L at 37°C. Fluorescence at 488 nm was monitored every

150 s using a multimode detector.

HIV-1 RT was expressed in *E. coli* and purified by using a HiTrap Ni affinity column. The purified RT was dialyzed to reduce the concentration of imidazole from the elution buffer and then incubated with human rino virus (HRV) 3C protease to cleave an N-terminal hexahistidine tag. The protein was further purified by nickel-coordinated nitrilotriacetic acid (Ni-NTA) to remove the uncleaved protein and HRV 3C protease. The RT was dialyzed against a buffer of 50 mM Tris-HCl at pH 7.5 and 200 mM NaCl and was stored at -20°C with adding 50% (v/v) glycerol.

Assessment of Cytotoxicity [3-(4,5-Dimethylthiazol-2-yl)-2,5-diphenyltetrazolium bromide] (MTT) assay was carried out with 293T cell line. First, 100 μ L medium (RPMI-1640) supplemented with 10% fetal bovine serum (FBS) containing 2% dimethylsulfoxide (DMSO) was loaded in a 96-well plate, and 200 μ L medium with 10% FBS and 2% DMSO containing test compounds at a concentration of 200 μ M was added to the wells in the first column of the plate. Different concentrations of compound were prepared for the second, third and fourth columns. The final concentrations of these columns were 100, 50, 25 and 12.5 μ M, respectively. Second, 100 μ L 293T cells at a concentration of 2×10^5 /mL were added to the respective wells. The final concentration of DMSO in each well was 1%. Third, cells were incubated for 3 d at 37°C with 5% CO₂ atmosphere. A hundred micro liter of supernatant was removed from the cultured medium and 15 μ L MTT reagent for dye solution was added to each well and the cells were incubated for 1 h. Then, 100 μ L solution of stop mix was added, and the cells were incubated overnight at 4°C to sufficiently dissolve the dye. Finally, intensity of OD_{570/690} was measured by a spectrofluorometer.

Molecular Dynamics Simulation A computational model of HIV-1 RT domain was constructed from an X-ray crystal structure with Protein Data Bank code 3QIO.²³ Atom coordinates for the missing residues were generated by using Modeller9.9.²⁴ According to the results of the recent X-ray crystallographic studies on the complex of RNase H domain and its inhibitors,^{25–27} the RNase H domain contains two divalent metal ions at the center of the active site. Two Mn²⁺ ions in the crystal structure were replaced with Mg²⁺ ions. The protonation states of all of the ionizable residues were predicted by ProPKa program²⁸ in the presence of two Mg²⁺ ions at the active site. Atom charges of the compounds were determined from the electrostatic potential obtained from quantum chemical calculations, followed by the restrained electrostatic potential (RESP) fitting²⁹ in a similar manner to the previous studies.^{30–33} The atom charge for Mg²⁺ ion was setting to 1.54, which was also determined by the RESP method based on the calculated electrostatic potential obtained by QM/MM technique carried out in a similar manner to the previous work.²⁰ An active compound was combined with HIV-1 RT domain, referring the binding structure predicted in our previous work.²⁰ The compound-bound RT model was placed in a rectangular box and solvated with TIP3P water molecules,³⁴ with all of the crystal water molecules remaining. Periodic boundary conditions were applied to avoid the edge effect in all calculations.

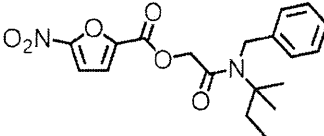
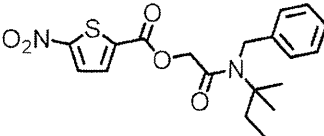
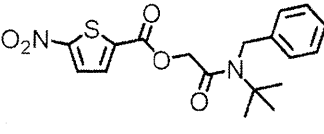
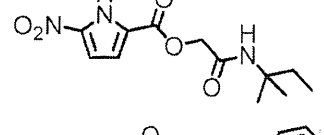
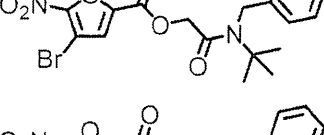
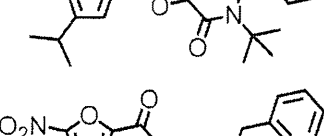
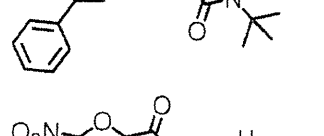
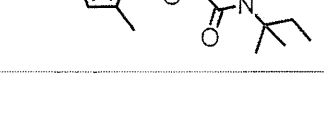
Minimizations and MD simulations were carried out using sander module of AMBER9.³⁵ The modified ff03 force field³⁶ was used as the parameters for molecular dynamics.

The cutoff distance for the long range electrostatic and van der Waals energy terms was set to 12.0 Å. The expansion and shrinkage of all covalent bonds connecting to hydrogen atom were constrained using the SHAKE algorithm.³⁷⁾ Energy minimization was achieved in three steps. Initially, movement was allowed only for water molecules. Next, compound and divalent metal ions were allowed to move in addition to the water molecules. Finally, all atoms were allowed to move freely. In each step, energy minimization was executed by the steepest descent method for the first 10000 cycles and the conjugated gradient method for the subsequent 10000 cycles. After a 0.1 ns heating calculation until 310K using the NVT ensemble condition, a 20 ns equilibrating calculation was executed at 1.0 atm and at 310K under the NPT ensemble condition, with an integration time step of 2.0 fs.

Results

Eight analogues of 5-nitro-furan-2-carboxylic acid ester were synthesized by converting the 5-nitro-furan moiety into other functional groups and examined for their RNase H inhibitory activities (Table 1). Compound **1** has a typical chemical structure showing an inhibitory potency for HIV-1 RNase H enzymatic activity. This compound bears nitro-furan ester core connecting to the pentyl- and benzyl-bound amide group. Replacement of furan with thiophene largely decreased compound potency (**2**, **3**). Conversion of furan into pyrrole also resulted in complete loss of compound potency (**4**). Attaching a halogen to the 4th position of furan exhibited a slight increase of inhibitory activity (**5**), while a hydrophobic or aromatic substitute resulted in loss of inhibitory potency (**6**, **7**). Introduction of even a small hydrophobic group at the 3rd position of furan decreased inhibitory activity (**8**).

Table 1. RNase H Inhibitory Activity and Cytotoxicity of the Derivatives Modulated at Nitro-Furan Moiety

Compound	Structure	IC ₅₀ (μM)	CC ₅₀ (μM)
1		8.4	74
2		>50	49
3		30.3	50
4		>50	86
5		6.6	3
6		>50	>100
7		>50	>100
8		25.7	76

Eight derivatives bearing 5-nitro-furan phenyl ester core were examined as shown in Table 2. A similar degree of inhibitory activity was observed for the analogs having a hydroxy group at the *meta* or *para* position of phenyl ring (9–11). While substitution of the hydroxy group with acetyl group showed a similar degree of inhibitory activity (12), substitution with ethyl-ester increased compound potency (13). Further, introduction of methoxy group at the *ortho* position also increased compound potency (14). The compound containing methoxy-carbonyl and methoxy groups at the *para* or *ortho* positions exhibited a fine inhibitory activity (15). Introduction of phenyl-methyl-amine at the *para* position also maintained compound potency (16).

Eleven derivatives bearing 5-nitro-furan ester core bound with benzyl-based substitutes were investigated as summarized in Table 3. Connection of a benzyl group without any additional functional substitute showed moderate inhibitory activity (17). Attaching nitro group, methoxy-ether, or *tert*-butoxy-ester exhibited slight changes in compound potency (18–20). Extension of alkyl chain caused no significant difference in inhibitory potency (21). However, addition of hydroxy group decreased inhibitory activity (22). Introduction of methoxy group further decreased compound potency regardless of the position of the group bound to phenyl ring (23–25). While connection of two methoxy groups improved compound potency (26), replacement of two methoxy groups by chlorides showed low inhibitory activity (27).

Six derivatives were synthesized by changing the ester bond

Table 2. RNase H Inhibitory Activity and Cytotoxicity of the Derivatives Bearing Phenyl Ester Core

Compound	-O-R	IC ₅₀ (μM)	CC ₅₀ (μM)
9		7.2	>100
10		8.2	24
11		9.1	>100
12		8.7	49
13		3.6	>100
14		3.1	>100
15		1.4	>100
16		3.8	>100

with carbonyl group as shown in Table 4. Ester linkage is disadvantageous for medicine because esterase digests the linkage and the drug concentration in a body decreases rapidly. Nitro-phenyl group was connected to the carbonyl carbon with changing the length of alkyl chain and the position of nitro group (28–30). None of the derivatives showed noticeable inhibitory activity. The ester linkage was replaced by an amide bond (31–33), in which hydroxy-methyl-benzyl, acetyl-methyl-benzyl, or bromo-methyl-benzyl was bound *via* a carbamoyl group. This modification also resulted in complete loss of compound potency.

Cytotoxicity was little or undetectable for most of the derivatives modulated at the nitro-furan moiety except for compound 5 (Table 1). No detectable cytotoxicity was also observed for most of the derivatives bearing nitro-furan-phenyl ester core (Table 2). It should be noted that highly active compounds, 14 and 15, showed no noticeable cytotoxicity at a concentration of 100 μM. In contrast, the analogs bearing ester core bound with benzyl-based substitute showed some degree of cytotoxicity (Table 3). Further, the analogs converted the ester into amide or ketone showed cytotoxicity in which CC₅₀ ranged from 9 to 32 μM (Table 4). Overall, in the measurement using 293T cells, half of the synthesized compounds showed noticeable cytotoxicity but almost all of the toxicity-detected compounds showed little RNase H inhibitory activity. Accordingly, the results of this assay suggest that active compounds have no significant cytotoxicity and the nitro-furan-phenyl ester skeleton is the most favorable among them from a cytotoxic viewpoint.

In order to examine the stability of the binding structure of a potent compound inside the active site of the target protein, MD simulation was performed for the complex of a synthesized derivative 15 and RNase H domain. MD simulation was carried out for 20ns and root mean square deviation (RMSD) relative to the structure after heating was calculated as shown in Fig. S1 of the supplemental information. The RMSD value showed a gradual increase up to 5ns and scarcely changed during later 15ns. Accordingly, the binding conformation of the complex was judged to be equilibrated. In order to extract the snapshot structure representing a typical binding mode of compound 15 and RNase H domain, the averaged structure was obtained using 2500 trajectories from the last 5ns of MD simulation. The RMSD between each trajectory and the average structure was calculated, and then one trajectory with the smallest RMSD value was determined to be the typical complex structure shown in Fig. 1a.

Two Mg²⁺ ions were held by the side chains of four acid residues; Asp443, Glu478, Asp498, Asp549, and the compound was stably bound to the active site without changing the binding mode during 20ns simulation. In the binding structure, the nitro-furan-ester core is especially, stably bound to two Mg²⁺ ions as shown in Fig. 1a. A stereo view of the binding structure is presented in Fig. S2 of the supplemental information. The oxygen atom on the furan ring is oriented toward the divalent metals. Nitro oxygen and carbonyl oxygen of the ester are strongly coordinated to the respective Mg²⁺ ions. Therefore, a large ring-shaped configuration of -Mg-O-N-C-O-C-C-O-Mg- is formed. The inter-atomic distance between two Mg²⁺ ions is 3.8 Å. The distance between the nitro oxygen atom and one Mg²⁺ ion is 1.9 Å, and that between carbonyl oxygen and the other Mg²⁺ ion is also 1.9 Å. Figure

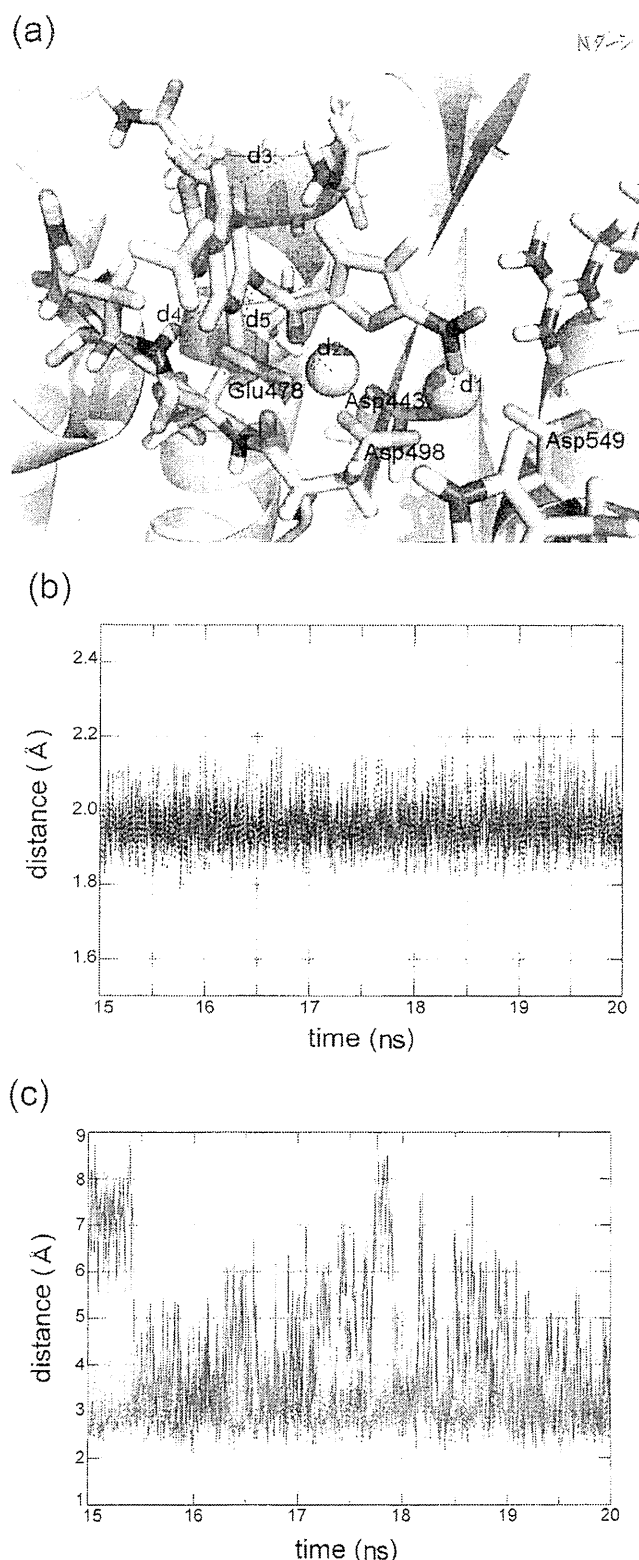


fig. 1. (a) Binding Structure of an Active Compound to the RNase H Domain, Obtained by MD Simulation

Compound and several polar residues are shown in stick representation. Two Mg²⁺ ions are denoted by spheres. (b) Changes in the distances between nitro oxygen and Mg²⁺ ion (d₁; solid line) and between carbonyl oxygen and another Mg²⁺ ion (d₂; dotted line) for the last 5 ns of MD simulation. (c) Changes in the distances between methoxy oxygen and amino hydrogen of Asn474 (d₃; solid line), between ester oxygen and amide hydrogen of main chain of Gln500 (d₄; broken line), and between ester oxygen and C α hydrogen of Ser499 (d₅; dotted line) for the last 5 ns of MD simulation.

1b shows the changes of these two distances for the last 5 ns of MD simulation. These graphs clearly indicate that the interaction of oxygen atom and Mg²⁺ ion is quite strong and that the oxygen-Mg interaction is essentially important for the binding of potent compound.

Methoxy-carbonyl and methoxy groups connected to phenyl stick out from the binding pocket. The distance between methoxy oxygen and hydrogen atom of amino group of Asn474 was monitored as shown in Fig. 1c. The distance largely fluctuates during the simulation and the interaction is not so steady. Hence, there is much room for improvement in this region. The oxygen atom at the ester bond has noticeable interactions with the amide group of main chain of Gln500. The change of the distance between the ester oxygen and the hydrogen atom of the amide group is shown in Fig. 1c. No abrupt, large change is observed in the distance. Therefore, the interaction contributes to stabilizing the binding of the potent compound. The distance between the ester oxygen and the C α hydrogen atom of Ser 499 was also monitored. The distance shows no large change for the last 5 ns of simulation, which suggests the stability of the binding of the ester part with RNase H domain. Consequently, it is confirmed from the MD simulation that an active compound **15** is stably bound to the active site of the RNase H domain with coordinating to two divalent metal ions and making supportive interaction at the ester part.


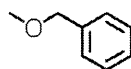
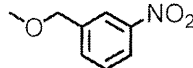
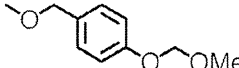
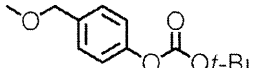
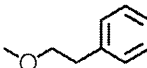
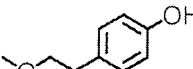
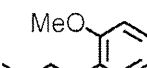
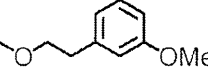
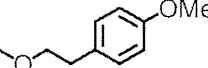
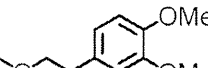
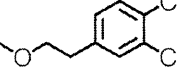
Discussion

According to the data summarized in Table 3, it is suggested that various kinds of functional groups connected to the benzyl ring have little interaction with the RNase H domain and that the functional group-binding region is located outside the binding pocket and is exposed to the solvent. Further, a comparison of inhibitory activity between compounds **17–20** and compounds **21–27** suggests that the length of alkyl chain connecting to phenyl ring has a significant influence on the difference in compound potency. That is, the longer alkyl chain in compounds **21–27** is less favorable in terms of both inhibitory activity and cytotoxicity. This indicates that a strategy to increase the inhibitory activity is to position the substitute closer to the nitro-furan group. The conversion may allow the aromatic ring or substitute to interact with the target protein inside the binding pocket.

A comparison of inhibitory activities of compounds in Tables 2 and 3 indicates that the introduction of phenyl-ester connected to nitro-furan shows higher compound potency than that of benzyl-ester. This is consistent with the findings described above paragraph and supports the notion that the compound potency increases when the position of the substitute connected to the ester linkage is closer to the nitro-furan. The incorporation of polarized substitutes like methoxy, hydroxy, methoxy-carbonyl, or ethoxy-carbonyl group is effective to increase the compound potency. In particular, the introduction of methoxy group at the *ortho*-position of phenyl ring effectively increases the inhibitory activity.

All the compounds in Tables 2 and 3 have the ester linkage. The data summarized in Table 4 clearly indicate that conversion of the ester linkage into carbonyl and/or amide bond results in loss of inhibitory potency. Both bonds will be likely to make the chemical to be in a straight configuration. If a compound has a straight form, the side part of the compound

Table 3. RNase H Inhibitory Activity and Cytotoxicity of the Derivatives Bearing Ester Core Bound with Benzyl-Based Substitute

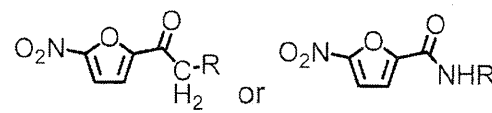
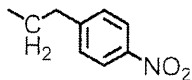
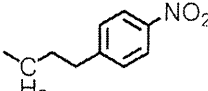
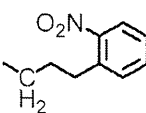
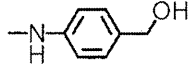
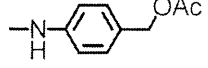
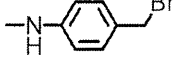
			
Compound	-O-R	IC ₅₀ (μM)	CC ₅₀ (μM)
17		5.4	38
18		5.0	>100
19		5.8	75
20		4.5	>100
21		5.1	57
22		7.9	39
23		14.2	42
24		18.6	36
25		12.5	36
26		8.5	51
27		17.4	64

will collide with the inside wall of the binding pocket of the RNase H domain. Accordingly, compounds are hardly combined with the binding pocket.

The conversion of the nitro-furan group into pyrrole drastically decreases the inhibitory activity while conversion to nitro-thiophen maintains the activity (Table 1). This indicates that a nitro-furan or nitro-thiophene core is indispensable for inhibitory potency. The characteristic property of nitro-furan is its large electric polarity. Oxygen atoms are negatively charged and these oxygen atoms will be coordinated to divalent metal ions at the RNase H active site. The attachment of non-polar substitute to furan results in decrease of compound potency. Accordingly, the 3rd and 4th positions of furan become close to the residues inside the RNase H active site.

RNase H of HIV-1 exerts its enzymatic activity by incorporating divalent metal ions at the reaction site.^{38,39} It had been controversial how many metal ions were required at the RNase H reaction site to exert its enzymatic activity.⁴⁰ A

Table 4. RNase H Inhibitory Activity and Cytotoxicity of the Derivatives Converted the Ester Bond into Other Kinds of Linkages

			
Compound	-CH ₂ -R or -NH-R	IC ₅₀ (μM)	CC ₅₀ (μM)
28		>50	11
29		>50	17
30		>50	9
31		>50	29
32		>50	27
33		>50	32

theoretical study by De Vivo *et al.* suggested that the presence of two divalent metal ions is essential for RNase H activity and that two metal ions act cooperatively with facilitating the binding of a substrate and catalyzing the enzymatic reaction.⁴¹ This theoretical finding strongly suggests double coordination of divalent metal ions at the RNase H domain. Crystal structures on the complex of the RNase H domain and its inhibitor were successively reported from three different research groups.^{23,25-27} All of the crystal structures ever reported showed the presence of two metal ions at the active site. One of the divalent metal ions was held deep inside the binding pocket of the RT RNase H domain with making coordination bonds to three carboxyl groups of Asp443, Glu478 and Asp498. The other was fixed with making coordination bonds to two carboxyl groups of Asp443 and Asp549. The distance between two metal ions was about 4 Å. Every inhibitor in crystal structures was revealed to have a similar binding mode. That is, inhibitors are stabilized with forming coordination bonds to both metal ions. Accordingly, it is highly probable that the chemical compounds showing RNase H inhibitory activity examined in this study are also coordinated to two divalent metal ions. Hence, negatively charged oxygen atoms of the nitro group, furan, and carbonyl group are aligned in a straight form. This negatively charged region will be attached to the divalent metal ions.

The binding structure deduced from MD simulation indicates that ether oxygen at the ester bond has an interaction with a polar residue, Ser499, which is located at the deep inside of RNase H domain. This residue would have little influence on the function of RNase H. Therefore, one of the

designs to improve inhibitory activity is to modify the compound to bear some polar functional group that enables a strong interaction with Ser499. In order to enhance the binding affinity of the compounds with RNase H active site, the incorporation of a polar functional group bound to phenyl ring is one of the possible conversions of our derivatives. The distance between methoxy group and the amine of Asn474 largely fluctuated during MD simulation. If the interaction with Asn474 is enforced, compound will be more stably combined with the RNase H domain.

Conclusion

More than 30 chemical compounds were synthesized for developing the inhibitors of RNase H activity of HIV-1 reverse transcriptase. Inhibitory potency of RNase H enzymatic activity was measured in a biochemical assay with a real-time fluorescence monitoring method. The active compounds found in our previous studies commonly bear nitro-furan ring connecting to hydrophobic region *via* an ester linkage. Conversion of the nitro-furan group into pyrrole drastically decreased the inhibitory activity while conversion into nitro-thiophene maintained the compound potency. This means that the structural basis of nitro-furan or nitro-thiophene is indispensable for inhibitory activity. An improvement in compound potency was observed when a phenyl-ester moiety was connected to the nitro-furan and further methoxy-carbonyl and methoxy groups were bound to the phenyl ring. No notable change in inhibitory potency was observed when benzyl-ester based substitute was connected to nitro-furan. Modulation of ester linkage resulted in complete loss of compound potency. Molecular dynamics simulation was performed to examine the stability of the binding structure of a synthesized active compound to RNase H domain. It was demonstrated that a potent compound was stably bound to the active site with establishing strong coordinate bonds with divalent metal ions located at the active site. The present study provides important information for designing prospective chemical structures inhibiting HIV-1 RNase H activity.

Acknowledgments This work was supported by a Health and Labor Science Research Grant for Research on Publicly Essential Drugs and Medical Devices from the Ministry of Health and Labor of Japan. A part of this work was also supported by a Grant-in-Aid for Scientific Research (C) from Japan Society for the Promotion of Science (JSPS). Theoretical calculations were performed at the Research Center for Computational Science, Okazaki, Japan and at the Information Technology Center of the University of Tokyo and also by the high-performance computer system at Institute for Media Information Technology in Chiba University.

References

- Goody R. S., Müller B., Restle T., *FEBS Lett.*, **291**, 1–5 (1991).
- Ren J., Stammers D. K., *Virus Res.*, **134**, 157–170 (2008).
- Andréola M. L., De Soultrait V. R., Fournier M., Parissi V., Desjobert C., Litvak S., *Expert Opin. Ther. Targets*, **6**, 433–446 (2002).
- Klumpp K., Mirzadegan T., *Curr. Pharm. Des.*, **12**, 1909–1922 (2006).
- Tramontano E., *Mini Rev. Med. Chem.*, **6**, 727–737 (2006).
- Tanese N., Telesnitsky A., Goff S. P., *J. Virol.*, **65**, 4387–4397 (1991).
- Telesnitsky A., Goff S. P., *EMBO J.*, **12**, 4433–4438 (1993).
- Borkow G., Fletcher R. S., Barnard J., Arion D., Motakis D., Dmitrienko G. I., Parniak M. A., *Biochemistry*, **36**, 3179–3185 (1997).
- Tramontano E., Esposito F., Badas R., Di Santo R., Costi R., La Colla P., *Antiviral Res.*, **65**, 117–124 (2005).
- Tarrago-Litvak L., Andréola M. L., Fournier M., Nevinsky G. A., Parissi V., de Soultrait V. R., Litvak S., *Curr. Pharm. Des.*, **8**, 595–614 (2002).
- Cowan J. A., Ohyama T., Howard K., Rausch J. W., Cowan S. M., Le Grice S. F., *J. Biol. Inorg. Chem.*, **5**, 67–74 (2000).
- Haren L., Ton-Hoang B., Chandler M., *Annu. Rev. Microbiol.*, **53**, 245–281 (1999).
- Steitz T. A., Smerdon S. J., Jäger J., Joyce C. M., *Science*, **266**, 2022–2025 (1994).
- Nowtny M., Gaidamakov S. A., Crouch R. J., Yang W., *Cell*, **121**, 1005–1016 (2005).
- Nowtny M., Gaidamakov S. A., Crouch R. J., Yang W., *EMBO J.*, **25**, 1924–1933 (2006).
- Shaw-Reid C. A., Munshi V., Graham P., Wolfe A., Witmer M., Danzeisen R., Olsen D. B., Carrol S. S., Embrey M., Wai J. S., Miller M. D., Cole J. L., Hazuda D. J., *J. Biochem.*, **278**, 2777–2780 (2003).
- Hang J. Q., Rajendran S., Yang Y., Li Y., In P. W. K., Overton H., Parkes K. E. B., Cammack N., Martin J. A., Klumpp K., *Biochem. Biophys. Res. Commun.*, **317**, 321–329 (2004).
- Budihis S. R., Gorshkova I., Gaidamakov S., Wamiru A., Bona M. K., Parniak M. A., Crouch R. J., McMahon J. B., Beutler J. A., Le Grice S. F., *Nucleic Acids Res.*, **33**, 1249–1256 (2005).
- Fuji H., Urano E., Futahashi Y., Hamatake M., Tatsumi J., Hoshino T., Morikawa Y., Yamamoto N., Komano J., *J. Med. Chem.*, **52**, 1380–1387 (2009).
- Yanagita H., Urano E., Matsumoto K., Ichikawa R., Takaesu Y., Ogata M., Murakami T., Wu H. G., Chiba J., Komano J., Hoshino T., *Bioorg. Med. Chem.*, **19**, 816–825 (2011).
- Chan K. C., Budihis S. R., Le Grice S. F., Parniak M. A., Crouch R. J., Gaidamakov S. A., Isaaq H. J., Wamiru A., McMahon J. B., Beutler J. A., *Anal. Biochem.*, **331**, 296–302 (2004).
- Parniak M. A., Min K. L., Budihis S. R., Le Grice S. F., Beutler J. A., *Anal. Biochem.*, **322**, 33–39 (2003).
- Lansdon E. B., Liu Q., Leavitt S. A., Balakrishnan M., Perry J. K., Lancaster-Moyer C., Kutty N., Liu X., Squires N. H., Watkins W. J., Kirschberg T. A., *Antimicrob. Agents Chemother.*, **55**, 2905–2915 (2011).
- Marti-Renom M. A., Stuart A. C., Fiser A., Sánchez R., Melo F., Sali A., *Annu. Rev. Biophys. Biomol. Struct.*, **29**, 291–325 (2000).
- Kirschberg T. A., Balakrishnan M., Squires N. H., Barnes T., Brenda K. M., Chen X., Eisenberg E. J., Jin W., Kutty N., Leavitt S., Liclican A., Liu Q., Liu X., Mak J., Perry J. K., Wang M., Watkins W. J., Lansdon E. B., *J. Med. Chem.*, **52**, 5781–5784 (2009).
- Himmel D. M., Maegley K. A., Pauly T. A., Bauman J. D., Das K., Dharia C., Clark A. D. Jr., Ryan K., Hickey M. J., Love R. A., Hughes S. H., Bergqvist S., Arnold E., *Structure*, **17**, 1625–1635 (2009).
- Su H. P., Yan Y., Prasad G. S., Smith R. F., Daniels C. L., Abeywickrema P. D., Reid J. C., Loughran H. M., Kornienko M., Sharma S., Grobler J. A., Xu B., Sardana V., Allison T. J., Williams P. D., Darke P. L., Hazuda D. J., Munshi S., *J. Virol.*, **84**, 7625–7633 (2010).
- Li H., Robertson A. D., Jensen J. H., *Proteins*, **61**, 704–721 (2005).
- Cieplak P., Cornell W. D., Bayly C., Kollman P. A., *J. Comput. Chem.*, **16**, 1357–1377 (1995).
- Matsuyama S., Aydan A., Ode H., Hata M., Sugiura W., Hoshino T., *J. Phys. Chem. B*, **114**, 521–530 (2010).
- Sano E., Li W., Yuki H., Liu X., Furihata T., Kobayashi K., Chiba K., Neya S., Hoshino T., *J. Comput. Chem.*, **31**, 2746–2758 (2010).
- Ode H., Neya S., Hata M., Sugiura W., Hoshino T., *J. Am. Chem.*

- Soc.*, **128**, 7887–7895 (2006).
- 33) Ode H., Matsuyama S., Hata M., Neya S., Kakizawa J., Sugiura W., Hoshino T., *J. Mol. Biol.*, **370**, 598–607 (2007).
- 34) Jorgensen W. L., Chandrasekhar J., Madura J. D., Impey R. W., Klein M. L., *J. Chem. Phys.*, **79**, 926–935 (1983).
- 35) Case D. A., Darden T. A., Cheatham T. E. III, Simmerling C. L., Wang J., Duke R. E., Luo R., Merz K. M., *et al.*, "AMBER 9," University of California, San Francisco, 2006.
- 36) Katagiri D., Fuji H., Neya S., Hoshino T., *J. Comput. Chem.*, **29**, 1930–1944 (2008).
- 37) Ryckaert J.-P., Ciccotti G., Berendsen H. J. C., *J. Comput. Phys.*, **23**, 327–341 (1977).
- 38) Sarafianos S. G., Das K., Tantillo C., Clark A. D. Jr., Ding J., Whitcomb J. M., Boyer P. L., Hughes S. H., Arnold E., *EMBO J.*, **20**, 1449–1461 (2001).
- 39) Huang H., Chopra R., Verdine G. L., Harrison S. C., *Science*, **282**, 1669–1675 (1998).
- 40) Klumpp K., Hang J. Q., Rajendran S., Yang Y., Derosier A., Wong Kai In P., Overton H., Parkes K. E., Cammack N., Martin J. A., *Nucleic Acids Res.*, **31**, 6852–6859 (2003).
- 41) De Vivo M., Dal Peraro M., Klein M. L., *J. Am. Chem. Soc.*, **130**, 10955–10962 (2008).

Mechanism of Drug Resistance of Hemagglutinin of Influenza Virus and Potent Scaffolds Inhibiting Its Function

Hiroshi Yanagita,^{†,‡} Norio Yamamoto,^{‡,§,‡,*} Hideyoshi Fuji,[†] Xinli Liu,[†] Masakazu Ogata,[†] Mizuho Yokota,[†] Hiroshi Takaku,^{||} Hideki Hasegawa,[†] Takato Odagiri,[‡] Masato Tashiro,[‡] and Tyuji Hoshino^{†,*}

[†]Graduate School of Pharmaceutical Sciences, Chiba University, Inohana 1-8-1, Chuo-ku, Chiba 260-8675, Japan

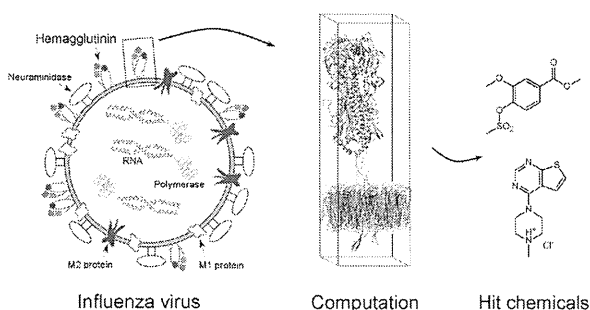
[‡]Influenza Virus Research Center and [†]Department of Pathology, National Institute of Infectious Diseases, 4-7-1 Gakuen, Musashimurayama, Tokyo 208-0011, Japan

[§]Department of General Medicine, Juntendo University School of Medicine, 2-1-1 Hongo, Bunkyo-ku, Tokyo 113-8421, Japan

^{||}Department of Life and Environmental Science, Chiba Institute of Technology, 2-17-1 Tsudanuma, Narashino-shi, Chiba 275-0016, Japan

Supporting Information

ABSTRACT: Highly pathogenic influenza viruses have become a global threat to humans. It is important to select an effective therapeutic option suitable for the subtypes in an epidemic or pandemic. To increase the options, the development of novel antiviral agents acting on targets different from those of the currently approved drugs is required. In this study, we performed molecular dynamics simulations on a spike protein on the viral envelope, hemagglutinin, for the wild-type and three kinds of mutants using a model system consisting of a trimeric hemagglutinin complex, viral lipid membrane, solvation waters, and ions. A natural product, stachyflin, which shows a high level of antiviral activity specific to some subtypes of influenza viruses, was examined on binding to the wild-type hemagglutinin by docking simulation. The compound potency of stachyflin is, however, easily lost due to resistant mutations. From a comparison of simulation results between the wild-type and the resistant mutants, the reason for the drug resistance of hemagglutinin was clarified. Next, 8 compounds were selected from a chemical database by *in silico* screening, considering the findings from the simulations. Inhibitory activities to suppress the proliferation of influenza virus were measured by cell-based antiviral assays, and two chemical scaffolds were found to be potent for an inhibitor. More than 30 derivatives bearing either of these two chemical scaffolds were synthesized, and cell culture assays were carried out to evaluate the compound potency. Several derivatives displayed a high compound potency, and 50% effective concentrations of two synthesized compounds were below 1 μ M.



Influenza viruses cause acute respiratory infection in humans that occasionally progresses to a severe pulmonary condition. Even seasonal epidemics account for 300,000 or more deaths per a year all over the world. Recently, the emergence of highly pathogenic avian and swine influenza viruses has become a global threat to humans. Avian influenza H5N1 virus infections have been reported since 2003,¹ and a pandemic of transmissible H5N1 virus is a serious concern for public health.² The recent outbreak of swine influenza subtype H1N1 resulted in considerable mortalities for infants and the elderly. While several anti-influenza drugs are currently approved, their effectiveness for pandemic viruses may be limited due to drug resistance. Therefore, the development of additional antiviral agents against influenza virus infection is needed.

The currently available anti-influenza drugs target one of two viral proteins: M2 protein and neuraminidase. M2 protein is embedded in the lipid membrane of the viral envelope and functions as an ion channel to pump protons into the viral particles. Amantadine and Rimantadine block the function of M2 protein by combining at the center of the channel or the side domain of this enzyme.^{3,4} Neuraminidase is a kind of spike protein sticking out on the viral particle surface. Neuraminidase causes the hydrolysis of neuraminic acid of the glycan of the host cell. Zanamivir, Oseltamivir, Peramivir, and Laninamivir have been used as neuraminidase inhibitors.^{5,6} Emergence of drug-resistant viruses has been reported for the above approved

Received: September 1, 2011

Accepted: January 4, 2012

Published: January 4, 2012

drugs. For example, resistance against Amantadine and Rimantadine was shown in the H3N2 and H1N1 viruses, and resistance against Oseltamivir was shown for the H1N1 virus.^{7–9} Since an RNA virus easily acquires amino acid mutations, the emergence rate of drug-resistant viruses is high. A drug-resistant virus is a serious issue in infectious diseases because a chemotherapeutic approach is restricted. In order to combat drug-resistant viruses, it is important to prepare many chemotherapeutic options and select an effective option suitable for subtypes in an epidemic. Accordingly, development of novel antiviral drugs that act on a target different from those of the currently approved drugs is needed.

A species of moss, *Stachybotrys s. RF-7260*, generates a unique natural product named stachyflin. Stachyflin was found to have strong antiviral activity against some subtypes of influenza viruses.^{10–12} The inhibitory mechanism of stachyflin is different from the inhibitory mechanism of the currently approved anti-influenza drugs. Stachyflin binds with hemagglutinin (HA) on the viral envelope and blocks conformational change of HA to prevent the lipid membrane of the viral envelope from merging with that of host cell. HA is one of the attractive targets of antiviral agents for the following reasons. First, HA is a key component in the viral infusion process that has no cellular counterparts and therefore has a potential advantage in selectivity and toxicity. Second, HA inhibitors will complement other currently approved drugs since they act on a different molecular target in the virus life cycle.

Stachyflin is highly effective for influenza virus of A/WSN/33 H1N1 subtype, and the 50% inhibitory concentration (IC_{50}) value for the WSN strain was reported to be 3 nM.¹² However, its inhibitory activity for other strains including other H1N1 virus strains is not so high, and its inhibitory activity is easily decreased by amino acid mutations of the virus. Since several amino acid mutations involved in drug resistance are not localized in one domain of HA, it is difficult to understand the mechanism of drug resistance caused by mutations straightforwardly. The chemical structure of stachyflin is complicated. Five rings merge to form a structure called the 3*H*-naphthopyrano-isoindol-3-one scaffold, and stachyflin also contains five chiral centers (Figure 1a). This complexity in its chemical structure is another reason for the difficulty in improving compound potency for stachyflin derivatives.

Yoshimoto and co-workers performed an experiment on resistance induction with stachyflin¹³ and demonstrated that K51R, K121E, S206L in the HA2 subunit and V176I in the HA1 subunit appeared in resistant viruses (Figure 1b). K51R and K121E mutations were suggested to be essential for drug resistance. They suggested from a docking simulation that stachyflin was bound to a position close to Lys51 or Phe110 of HA. This simulation, however, provided no clear explanation for the mechanism of drug resistance due to the above amino acid mutations. The mechanism of the drug resistance of HA should be clarified for producing promising inhibitory compounds.

In this study, we performed computational analysis, screening to find candidate compounds, a cell-based antiviral assay, and synthesis of analogue compounds in the following manner: (1) Molecular dynamics (MD) simulations were carried out for the wild-type and three kinds of variants containing amino acid mutations responsible for drug resistance in order to clarify the mechanism. (2) A point for designing a potential inhibitor was deduced from the concept of minimizing the influence of the drug-resistance-related conformational change of HA. (3) An *in*

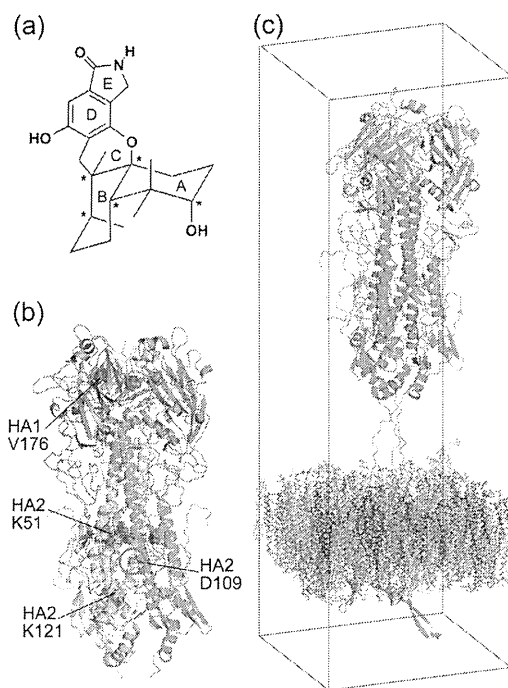


Figure 1. (a) Chemical structure of stachyflin. Stachyflin is composed of five complex rings and contains five chiral centers. The rings are labeled A–E, and chiral carbon atoms are marked by asterisks. (b) Structure of hemagglutinin in a trimer conformation. Spheres denote the residues introducing amino mutations in the respective mutants. The center residue targeted in the ligand docking simulation is indicated by a circle. (c) Calculation model of a complex of hemagglutinin trimer and lipid membrane. Hemagglutinin subunits HA1 and HA2 are colored blue and green, respectively. The membrane consists of 6 different kinds of lipid molecules, and its composition is presented in Supplementary Table S1. No water molecules or ions are shown for visual clarity.

silico screening was performed to find low-molecular-weight compounds showing inhibitory activity against HA, considering the above point and using the pharmacophore of stachyflin. (4) A cell-based assay was carried out to evaluate the inhibitory potencies of the compounds collected by the *in silico* screening. (5) Derivatives of the hit compounds found from the screening were synthesized, and their inhibitory activities were measured to elucidate the antiviral potency of the scaffold proposed in this work.

RESULTS AND DISCUSSION

Structural Difference in HA between the Wild-Type and Mutants. MD simulation was carried out for 30 ns to obtain the probable protein structure of HA in a trimer form for the wild-type and three mutants, using the model system containing a trimeric hemagglutinin and viral lipid membrane as shown in Figure 1c. The respective mutants contain the resistant mutations K51R and K121E in HA2 for mutant 1, V176I in HA1 and K51R, K121E in HA2 for mutant 2, and V176I in HA1 and K51R in HA2 for mutant 3. Root mean square deviation (rmsd) relative to the structure after heating is shown in Supplementary Figure S1. The rmsd value for the wild-type (Figure S1a) was scarcely changed during 30 ns. Each of the rmsd curves for the mutants (Figures S1b–d) shows a

gradual increase up to 15 ns and seems to be almost constant after 20 ns. Plots of rmsd in Figure S1 were obtained from the coordinates of main chain atoms of the whole HA. The N-terminal domain of the HA1 subunit is so flexible that rmsd values are considerably large. Hence, rmsd values were calculated again with respect to the main chain atoms of only the HA2 subunit with excluding the C-terminal region, aa 176–222. The rmsd curves only for HA2 in Supplementary Figure S2 also became constant after 20 ns for every model. Accordingly, protein conformations for the respective models were judged to be equilibrated.

Principal component analysis (PCA) in Supplementary Figure S3 indicates that the trajectory structures for the last 5 ns are in a single conformation for every model. The equilibration of the simulation is also confirmed from these PCA plots. In order to extract the plausible protein structure, the averaged structure was obtained using 500 trajectory structures from the last 5 ns of MD simulation. The rmsd between each trajectory structure and the average structure was calculated, and then one trajectory structure with the smallest rmsd value was determined to be the plausible protein structure. At a glance, there is no prominent difference among the 4 models in terms of shape of the trimer, conformation of the HA1 and HA2 subunits, or position of helices. Although no significant apparent change is seen in the backbone of HA, there appears a notable difference in the location of side chains. The differences in the side chain will be responsible for the change in binding affinity and inhibitory activity of inhibitors.

Binding of an Inhibitor to HA. By means of docking simulation, an inhibitor, stachyflin, was bound to the HAs, using the respective plausible protein structures obtained by MD calculations. In the wild-type HA, stachyflin was bound near Asp109 of the HA2 subunit (Figure 2). Hydrophobic interactions were observed between the B ring of stachyflin and Phe37 of HA1, between the C ring of stachyflin and Phe110 of HA2, and between the D ring and Leu113. Hydrogen bonds were formed between the O atom on the D ring of stachyflin and the amino group of Asn114 in HA2 and between the O atom on the E ring and the amino group of Asn117.

In mutant 2, stachyflin was bound to a location similar to that of the wild-type (Supplementary Figure S4c), while the docking simulation showed binding of stachyflin at the central space among three helices of the HA2 trimer in mutants 1 and 3 (Figures S4b and d). Judging from the binding affinity evaluated by ASP score function (Supplementary Table S2), the binding of stachyflin to the wild-type HA is the most stable. All of the mutants showed notable decrease in binding affinity compared to that of the wild-type.

An amino acid mutation of K51R in HA2 commonly appeared in the three mutants, suggesting that K51R was the primary mutation for drug resistance. Other mutations, K121E and V176I, will enhance the resistance. All of these amino mutations are, however, distant from the stachyflin binding site. Our MD simulation clearly indicated that inner helices of HA2 subunit were rotated (Figure 3a). One of the three inner helices, chain D in nomenclature in PDB 1RD8, was rotated by 10.8° in mutant 1 and by 15.0° in mutant 2 compared to the wild-type (Figure 3b). The amino group on the side chain of Lys51 makes a strong hydrogen bond with the hydroxy group of Thr107 of HA2 (Figure 3c). Arg is also a positively charged amino acid residue, but the length of the side chain is longer than that of Lys. When Lys is converted into Arg, the side chain

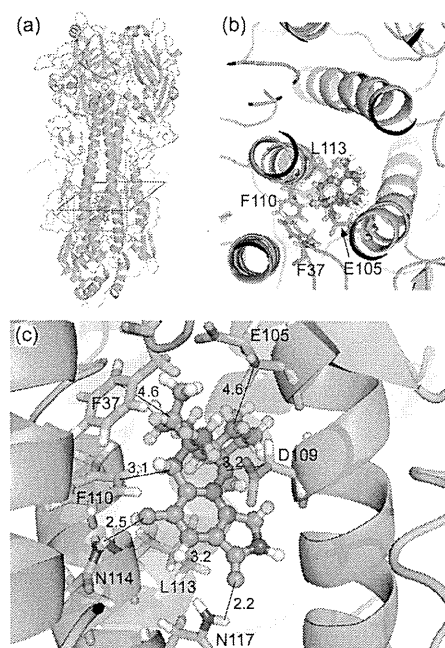


Figure 2. (a) Complex structure of stachyflin and hemagglutinin obtained by the ligand docking simulation. (b) Binding site of stachyflin viewed in a plane perpendicular to the helices of the HA2 subunit. (c) Binding mode of stachyflin, shown in a magnified view of the area indicated by a red frame in panel a. Stachyflin is bound to the space between two helices of HA2 subunit, making strong interaction with side chains of Asp109, Phe110, and Leu113. The interaction distances are in Å.

of the residue at codon 51 expands and pushes T107. The side chain of Thr107 serves as a lever to rotate the helix. The position of the side chain of Asp109 is largely deviated from that of the wild-type because of the closeness to Thr107. Lys121 has a strong interaction with the carboxy group of Asp18 of the HA1 subunit. When Lys is converted into Glu in the K121E mutation, the side chain of Glu121 and Asp18 of HA1 causes repulsion to increase the distance between them. This repulsion assists the helix rotation, and the deviation of Leu113 and Asn114 from the wild-type will be enhanced because of the closeness to Glu121. To monitor the helix rotation, the angle between the line connecting the $C\alpha$ and $C\beta$ atoms of Asp109 on the inner helix chain D and the line connecting the Asp109 $C\alpha$ atom on chain D and the Phe110 $C\alpha$ atom on another inner helix chain B was measured through the simulation as shown in Supplementary Figure S5. A significant angle change was observed after 10 ns for every model. The distances between the $N\zeta$ atom of Lys51 (or $C\zeta$ in K51R) of HA2 and the $O\gamma$ atom of Thr107 of HA2 and also between the $N\zeta$ atom of Lys121 (or $C\delta$ in K121E) of HA2 and $C\gamma$ of Asp18 of HA1 were monitored as shown in Supplementary Figure S6. Because HA is a trimer and there exist three HA1 and three HA2 subunits in the calculation models, three combinations of those interatomic distances were measured through the simulation. The distance plots in Figure S6 indicate that the interaction between the residues at codon 51 and codon 107 is quite stable in the wild-type HA. In contrast, some of these distances occasionally increased in the mutants. The distance between the residues at codon 121 of HA2 and at codon 18 of HA1 ceaselessly fluctuated in all

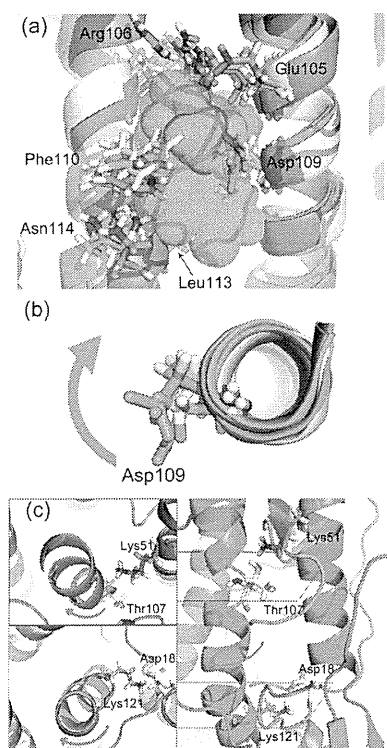


Figure 3. (a) Superposition of the hemagglutinin structures of mutants on that of the wild-type. The wild type is colored green and mutants 1, 2, and 3 are colored cyan, magenta, yellow, respectively. The binding area of stachyflin to the wild-type HA is shown in a mesh representation. There is no significant change in positions of helices. However, the amino acid mutations cause rotation of helices. The rotation angle is estimated from the position of $C\beta$ atom of Asp109, as shown in panel b. Thr107 in HA2 subunit and Asp18 in HA1 subunit are deeply involved in the helix rotation induced by K51R and K121E mutations, respectively, as shown in panel c. Two illustrations on the left side are depicted around the planes perpendicular to the helices and containing Thr107 or Lys121, respectively. The planes are indicated by blue and red frames in the right side illustration in panel c.

models. A strong interaction was, however, established at least for one combination of Lys121 and Asp18 in the wild-type.

The helix rotation pointed out above is the reason for the decrease in inhibitory activity of stachyflin to the resistant mutants. In the mutants, the side chains of Asp109 and Leu113 are displaced and occupy the space that stachyflin was bound to in the wild-type HA. The side chains of Phe110 and Asn114 are also displaced and move away from the stachyflin binding site as shown in Supplementary Figure S7. Therefore, stachyflin would not be bound to HA stably any more. The helix rotation in mutant 3 is small. This is naturally understood because the influence of V176I mutation in the HA1 subunit is slight. This finding suggests that some degree of flexibility is favorable to HA inhibitors for releasing the strain due to the helix rotation. Therefore, compounds bearing a complicated heteroring structure are disadvantageous. Instead, a single bond connection of separated ring domains can be a good chemical frame to maintain structural flexibility.

Conformational change accompanying helix rotation has been reported for other kinds of transmembrane proteins. For example, an X-ray crystallographic analysis of the human β 2

adrenergic G-protein-coupled receptor¹⁴ suggested that a rotational motion was observed for one of the transmembrane helices owing to the binding of a ligand for the receptor. An electron paramagnetic resonance measurement¹⁵ and a computational analysis¹⁶ indicated that light adsorption induced a conformational change of retinal chromophore in sensory rhodopsin and this conformational change caused the rotation of transmembrane helix TM1 to lead signal transduction of the sensory protein.

Search for Active Compounds. The natural product stachyflin possesses a unique pentacyclo structure in which each ring is labeled as A, B, C, D, and E, respectively. Rings AB are composed of a naphthol skeleton, and rings DE are composed of an indol frame. Ring C bears a pyran structure and connects rings AB and rings DE. Rings ABC are fused in *cis*-form, and the oxygen of pyran is bonded to the carbon at the junction of rings AB. Furthermore, stachyflin contains 5 chiral centers, in which all of the chiral carbons are located on rings AB. Therefore, the naphthol moiety and its connection to pyran make the chemical structure of stachyflin highly complicated. A hydroxy group and carbonyl oxygen are bound to the indol ring, which characterizes the electrostatic property of stachyflin. The hydroxy group of naphthol is another factor to characterize the polar feature of this natural product.

Eight chemical compounds were selected by an *in silico* screening using the pharmacophore of stachyflin (Table 1). All of the selected compounds were produced by organic synthesis and are available by purchase. The molecular weights of these compounds range from 304 to 341. Compound 1 bears two ester bonds and a benzofuran moiety corresponding to rings C and D of stachyflin in superimposition. Compound 2 bears a thieno-pyrimidine, which corresponds to rings D and E of stachyflin and a phenyl-cyclopentane corresponding to rings A and B. Two benzene rings are connected *via* a dichloromethyl-carbonyl group in compound 3. Methylbenzoic acid methyl-ester in compound 4 corresponds to rings D and E, and dimethyl-diazolane is connected by a sulfonyloxy group. Thieno-pyrimidine in compound 5 corresponds to rings D and E, and another thiophene corresponds to ring A. The molecular weight of compound 6 is the largest among the selected compounds, and methylester-benzene corresponds to rings D and E and pyridyl-triazole corresponds to rings A and B. Compound 7 bears a seven-membered ring containing two nitrogen atoms. Hydroxybenzene in compound 8 corresponds to ring B of stachyflin.

Assay for Antiviral Activity. The 8 selected compounds were tested in an influenza virus cell culture assay (Table 1). Compounds 4 and 5 were found to have significant antiviral activity ($EC_{50} < 5 \mu M$). Although compound 2 was the most highly potent with an EC_{50} of $3 \mu M$, compound 2 exhibited significant cytotoxicity at a concentration of $6 \mu M$, measured by an MTT assay with MDCK cells. Since compounds 4 and 5 showed no noticeable cytotoxicity, these two compounds were chosen as the structural core in the next step for organic synthesis.

The binding modes of compounds 4 and 5 to the wild-type HA were predicted by performing docking simulation. The most probable docking structures are shown in Figure 4a and b, which were determined from the score ranking for 50 docking poses. The two compounds are bound to almost the same position as stachyflin is. That is, these compounds are located not in the central space of HA2 trimer but at a position in the middle of two helices of the HA2 subunit. The calculated

Table 1. Structures and Inhibitory Activities of the Chemical Compounds Obtained through an *in Silico* Screening

Compound	Structure	Superimposition ^{a)}	EC ₅₀ (μM)	CC ₅₀ (μM)
1			9.0	> 60
2			3.0 >	5.9
3			> 32	> 60
4			4.4	> 60
5			4.9	> 60
6			17.9	> 60
7			31.4	> 60
8			14.9	> 60

^aStachyflin is depicted in green stick representation, while compounds are blue.

binding affinities of these two compounds in ASP score are lower than that of stachyflin (TSupplementary table S2) but higher than that in the cases of stachyflin bound to the three kinds of mutants.

Synthesis of Analogue Compounds. Compound 4 bears a structural core of vanillic acid. Based on the vanillic acid methylester core, 22 derivatives from compound 4 were synthesized as shown in Table 2, where the functional group at the fourth position of the benzoic acid was modulated. A highly potent compound (9) was found in the analogues in which methylsulfonyl was connected to the fourth position. The incorporation of benzyl or methylphenyl (10, 12) showed no inhibitory activity, while moderate activity was observed in case of phenyl only (11). This means that a small chemical group is favorable for the substitute connecting *via* the sulfonyloxy group. Conversion of the sulfonyl group into an ester bond (13–15) resulted in complete loss of compound potency, regardless of the size of the substitutes connected to

the ester. Substitution of the sulfonyl group by an alkyl chain (16–20) resulted in loss of inhibitory activity. Only compound 18 in which the sulfonyl group was substituted by benzyl showed slight inhibitory activity. Then the effect of addition of functional groups to the benzyl (21–28) was surveyed. Compound 22 containing an oxybenzyl group at the *para*-position of the benzyl exhibited high compound potency. The inhibitory activity was maintained with the addition of methoxy or trifluoromethyl at the *para*-position, while the incorporation of other kinds of functional groups (23–25) or the addition of trifluoromethyl at the *ortho*- or *meta*-position (27, 28) resulted in loss of inhibitory activity. Conversion of the sulfonyloxy group into an amino group (29, 30) was tested. None of the derivatives showed noticeable increase in compound potency.

Compound 5 bears a heteroring core of thieno-pyrimidine, and a dimethyl-aminy-thienyl group is connected to the heteroring *via* amine. Keeping the heteroring core, 9 derivatives from compound 5 were synthesized as shown in Table 3. The

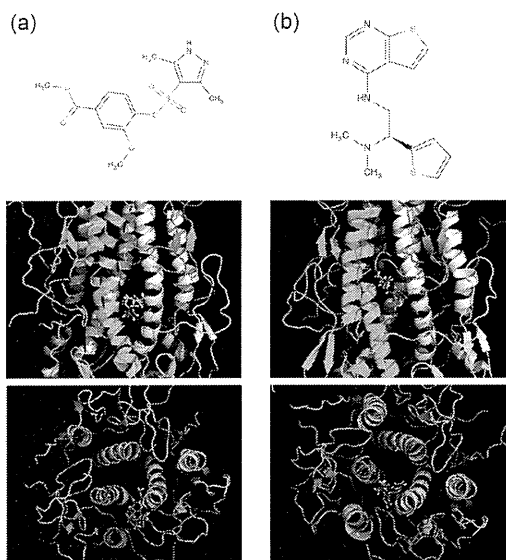


Figure 4. Hit chemicals found through *in silico* screening: (a) compound 4 and (b) compound 5. Top: chemical structure. Middle: binding site of the compound predicted by the docking simulation. Bottom: binding position of the compound viewed from the direction of subunit HA1.

introduction of benzyl *via* amine group (31) resulted in an increase in inhibitory activity. In contrast, conversion into dimethylamine (32, 33) resulted in loss of compound potency. Interestingly, while conversion into methyl-piperazine (34) resulted in a decrease in inhibitory activity, its hydrochloride salt (35) exhibited a high compound potency. Phenyl-piperazine (36) also exhibited a considerably high inhibitory activity. The conversion of thiophene of compound 5 into benzene (37) exhibited a high compound potency, while its chiral analogue (38) showed no inhibitory activity. This chiral-selective compound potency was confirmed by substitution of a Boc protection group (39) for the dimethylamine of compound 37.

Actions of Active Compounds for Blocking HA. Fusion of the membrane is an essential process in the entry of influenza virus into the host cell. HA mediates this process through two functions in the early stage of the viral life cycle.¹⁷ One is anchoring at sialylated glycoprotein receptors on the cell membrane surface. The other is the low-pH induced conformational change that initiates the exposure of a fusion peptide, a hydrophobic N-terminal segment buried in the HA trimer interface, to be inserted into the endosomal membrane. Stachyflin is assumed to block this fusogenic process of HA.^{12,13} Indeed, in the predicted binding structure shown in Figure 2, stachyflin is combined with HA with the formation of two strong hydrogen bonds and three strong aromatic ring-involved hydrophobic interactions.

Several other compounds blocking the fusogenic activity of HA have been identified.^{18–22} An active compound¹⁸ bears a naphthoquinone skeleton, which is commonly seen in stachyflin as rings AB. Another compound¹⁹ contains a quinolizin moiety connected to a benzamide skeleton, and a one-step virus growth experiment indicated that this compound mainly inhibited virus proliferation at the early stage of the replication cycle. Therefore, a quinoline skeleton is one of the effective chemical cores for binding to HA. A compound

containing piperidine connected to trifluoro-methylbenzoyl also showed high inhibitory activity for influenza virus replication.²⁰ Ligand docking calculation suggested that this compound was bound to a site near Phe110 of the HA2 subunit, which is almost identical to the binding site of stachyflin obtained in this work as shown in Figure 2. A compound analogue to podocarpic acid was identified as an inhibitor of type A viruses²¹ and showed a high inhibitory activity especially for Kawasaki strain but was not so sensitive to WSN strain. In contrast, some recently identified blockers are targeted at another domain of HA.^{23,24} Some peptides mimicking sialic acid were shown to inhibit the entry of viruses into host cells, attached to the receptor-binding site of HA.²³ Synthesized macromolecules containing three sialyllactoses linked with trisphenol or trisamine were reported to inhibit viral replication, combined with the receptor-binding site of HA.²⁴ Recently, an HA inhibitor bearing a benzenesulfonamide core was identified through structural modifications of a salicylamide derivative.²⁵ It is interesting to note that the chemical structure of this agent resembles that of compound 9 in Table 2 to some extent.

In most of the active compounds, susceptibility varies among strains of influenza viruses and the inhibitory activity is drastically decreased due to the acquisition of resistant mutation. Our MD simulation demonstrated that the rotation of helices is the reason for the reduction of compound potency. Due to the increase in performance of computers and the development of calculation methodology, several computational analyses have recently been carried out.^{26–32} Quantum mechanical calculations using the fragment molecular orbital method were used to investigate the role of key amino acid residues in recognizing sialoglycoproteins on the host cell surface²⁶ or in combining with neutralizing monoclonal antibodies.²⁷ Huge MD simulations were performed to examine the interaction between HA and sialoglycans²⁸ and clarify the reason for mutations at the receptor-recognizing site.²⁹ MD simulations were also employed to evaluate the binding free energy³⁰ and to interpret the difference in receptor specificity.³¹ A computational approach was further demonstrated to be quite helpful for designing protein peptides that strongly inhibit the function of HA.³²

Pharmaceutical Properties of Hit Chemicals. Since stachyflin exhibits a highly potent anti-influenza activity for the wild-type WSN strain and is a challenging synthetic target due to its unique alkaloid structure, two research groups have so far attempted total synthesis of stachyflin. The first total synthesis of racemic (\pm)-stachyflin was reported by Taishi *et al.*,¹¹ in which the characteristic structure of 5 heterorings was built one by one in 29 steps. The first enantioselective total synthesis of (+)-stachyflin was recently achieved by Watanabe *et al.*,³³ utilizing an acid-induced domino epoxide-opening, rearrangement, cyclization reaction.³⁴ These synthetic studies suggest the possibility for producing stachyflin analogues and encourage the development of stachyflin-based antiviral agents. The complexity in synthesis is, however, disadvantageous from the viewpoint of productivity in manufacturing. Carey and co-workers analyzed the reactions used for the preparation of drug candidate molecules,³⁵ surveying 128 compounds produced in the departments of process chemistry of three major pharmaceutical companies. According to their analysis, the average number of chemical steps for synthesizing one candidate is 8.1. Compounds containing a chiral center account for about half of the 128 molecules. Therefore, the structural

Table 2. Structures and Inhibitory Activities of the Synthesized Analogues to Compound 4, Which Bears a Vanillic Acid Core^a

Compound	X	R	Temp. (°C)	Time (h)	Yield (%)	EC ₅₀ (μM)
9		OSO ₂ Me	rt	3	71	0.9
10	OH	OSO ₂ CH ₂ Ph	rt	3	75	>10
11		OSO ₂ Ph	rt	6	81	7.0
12		OSO ₂ <i>p</i> -MeC ₆ H ₄	rt	6	82	>10
13	OH	OCOMe	rt	3	35	>10
14		OCOCH ₂ Cl	rt	3	66	>10
15		OCOPh	reflux	3	80	>10
16	OH		reflux	24	93	>10
17		OCH ₂ <i>t</i> -Bu	reflux	72	21	>10
18		OCH ₂ Ph	rt	8	81	8.3
19		OCH ₂ CH ₂ Ph	reflux	24	70	>10
20		OCH ₂ (CH ₂) ₂ Ph	reflux	24	91	>10
21	OH	OCH ₂ <i>p</i> -MeOC ₆ H ₄	rt	12	72	8.1
22		OCH ₂ <i>p</i> -BnOC ₆ H ₄	rt	12	83	2.5
23		OCH ₂ <i>p</i> -NO ₂ C ₆ H ₄	rt	12	67	>10
24		OCH ₂ <i>p</i> -FC ₆ H ₄	rt	12	88	>10
25		OCH ₂ 2,3,4,5,6-F ₅ C ₆	rt	12	82	>10
26		OCH ₂ <i>p</i> -CF ₃ C ₆ H ₄	rt	12	79	8.2
27		OCH ₂ <i>o</i> -CF ₃ C ₆ H ₄	rt	12	76	>10
28		OCH ₂ <i>m</i> -CF ₃ C ₆ H ₄	rt	12	68	>10
29	NH ₂	NHCH ₂ Ph	rt	12	54	8.5
30		N(CH ₂ Ph) ₂	rt	12	27	>10

^aCondition: (a) K₂CO₃, R-Cl, CH₃CN, temp, time, 21–93%.

core of stachyflin would not be suitable for scale-up synthesis in terms of the number of synthetic steps and the number of chiral centers. In this study, we provided two scaffolds exhibiting antiviral activity. Most of the compounds shown in Tables 2 and 3 were synthesized within 3 steps, except for compounds 37–39. Compounds 37–39 include chiral centers, and the synthesis of these compounds was achieved at most within 8 steps. Accordingly, the proposed scaffolds are feasible for diverse modulation of functional groups and then ones of the chemical bases for the development of HA inhibitors.

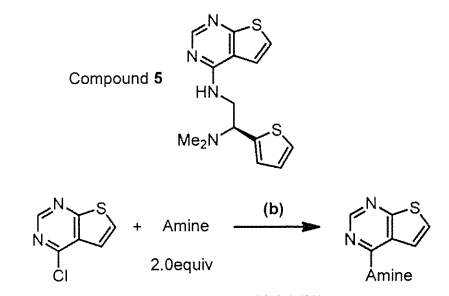
A requirement of antiviral drugs in clinical use is inhibitory activity for a broad range of viral strains. We tested the potency of several compounds synthesized in this study using A/Vietnam/1194/2004 (H5N1) strain,³⁶ which causes severe pathological conditions for humans and is one of the viruses attracting keen concern for the threat of a pandemic. A cell-based antiviral assay indicated that compounds 31 and 39 were effective for this H5N1 type virus with IC₅₀ values of 0.2 and 5.2 μM, respectively. This suggests that the scaffolds found in this study will maintain compound potency over different types of influenza viruses.

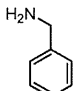
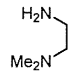
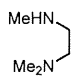
Plan of the Design of Potent Agents. In the *in silico* screening carried out in this study, 4 features, *i.e.*, hydrophobic region, hydrogen-bond donor, hydrogen-bond acceptor, and aromatic ring, were monitored for pharmacophore. Hit chemical compound 4 is compatible with stachyflin in the

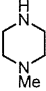
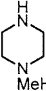
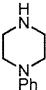
three features of aromatic ring, hydrophobic region, and hydrogen-bond acceptor. Hit chemical compound 5 is compatible in all four features. All of the 8 selected compounds are compatible with stachyflin at least in two features, aromatic ring and hydrogen-bond acceptor. That is, these two features are commonly observed in pharmacophores of all selected compounds. This suggests that aromatic ring and hydrogen-bond acceptor are indispensable for inhibitors analogous to stachyflin. From the viewpoint of compatibility in the pharmacophore, compound 5 is the most advantageous for an HA inhibitor. In the binding modes of compounds 4 and 5 to the wild-type HA shown in Figure 3, compound 4 generated three hydrogen bonds with HA. In contrast, one hydrogen bond was observed between compound 5 and HA. The binding position of compound 5 is considerably close to that of stachyflin. These findings in binding mode suggest that the shape complementarity between compound 5 and the binding site in HA is high, while electrostatic complementarity is more significant in the binding of compound 4.

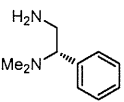
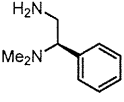
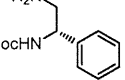
Methylester of compound 4 corresponds to carbonyl oxygen on ring E of stachyflin, and methoxy corresponds to the hydroxy group bound to ring D. It should be noted that rings DE of stachyflin compose a large flat region and that the vanillic acid core of compound 4 mimics the flat region and the distribution of polar atoms. Diazolane of compound 4 is compatible with ring A of stachyflin, and amine on the

Table 3. Structures and Inhibitory Activities of the Synthesized Analogues to Compound 5, Which Bears a Thieno-pyrimidine Core^a



Compound	Amine	Yield (%)	EC ₅₀ (μM)
31		45	3.6
32		62	>10
33		43	>10

34		54	>10
35		28	0.6
36		82	4.6

37		48	2.0
38		32	>10
39		7	4.8

^aCondition: (b) amine, NaOH, THF, reflux, 6 h.

diazolane corresponds to the hydroxy group bound to ring A. Compound 9 in Table 2, in which diazolane is replaced by methoxy, shows a considerably high inhibitory activity. Therefore, a polar group at the position of the diazolane is not necessarily required to maintain compound potency.

Sulfur and nitrogen atoms of thieno-pyrimidine moiety of compound 5 mimic the charge distribution of rings DE. It is notable that thieno-pyrimidine also composes a large flat

region. Another thiophene and dimethylamine are compatible with rings A and B of stachyflin, respectively. The high inhibitory activity of compound 35 in Table 3 suggests that thiophene is not necessarily required to maintain compound potency. This finding provides a sound explanation for the high inhibitory activity of compound 9. Accordingly, the region of ring A of stachyflin is not so important for inhibitory activity. Instead, the flat region at rings DE and the charge distribution on the flat region are essential for compound potency.

Compound 9 and 35 were docked to the wild-type HA and the three mutants in the same manner as stachyflin was. The predicted binding structures in Supplementary Figure S8 indicate that the binding site of compound 9 changed among the models. In contrast, compound 35 was bound to almost the same location among all models. The thieno-pyrimidine moiety is positioned near D109. This position is, however, different from that of stachyflin. The sizes of compounds 9 and 35 are small compared to stachyflin and compounds 4 and 5. Hence this smallness may be a reason for the incompatibility of the binding mode. To produce potent compounds appropriately fitted to the domain between inner helices of HA, compounds 9 and 35 should be converted with retention of the vanillic acid core and/or the thieno-pyrimidine moiety and with attachment of some chemical group containing a chiral center at the opposite side to cling to the helix round surface.

METHODS

Molecular Dynamics Simulation. Information on the structural difference between the wild-type HA and the mutants is essential for clarifying the reason why some amino acid mutations in HA diminish the inhibitory activity of stachyflin. The initial structure of the wild-type HA of WSN strain was constructed by homology modeling using Modeler ver. 9.4.³⁷ The multiple-alignment technique was employed, where the X-ray crystal structures of A/Puerto Rico/8/1934 H1N1 with PDB codes 1RVZ and 1RU7³⁸ and A/Brevig Mission/1/1918 H1N1 with code 1RD8³⁹ were selected for references in modeling. Homology modeling was also performed to build the initial structures for variants; K51R and K121E mutations were introduced in the HA2 subunit in mutant 1, V176I in HA1 and K51R, K121E in HA2 in mutant 2, and V176I in HA1 and K51R in HA2 in mutant 3. A lipid bilayer of 100 Å × 100 Å was generated by using an in-house software GLYMM implemented in VMD ver. 1.8⁴⁰ for the purpose of embedding the C-terminal side of HA2 subunit into the lipid membrane mimicking the viral envelope. The composition of lipid molecules in the membrane was set to be as compatible as possible with the composition of lipid molecules in the influenza viral envelope, as shown in Supplementary Table 1. Judging from the prediction results with UniProtKB,⁴¹ amino residues 186–206 were assumed to be the transmembrane region embedded in the viral envelope. It is natural to consider that an α helix structure is formed in the transmembrane region. However, there is no experimental ground for the formation of an α helix in this region. Accordingly, this region was set to have no secondary structure, that is, to be in a strand form in the initial structure of the present simulations. In our preliminary calculation without embedding the C-terminal side of HA2 subunit into the lipid membrane, each helix in HA2 gradually changed its conformation to separate itself from other helices. HA trimer was converted from a closed shape to an open one with the progress of simulation. The motion of the C-terminal region of HA2 was large in the preliminary calculation, which seemed to be a cause of structural instability and became a trigger for the drastic conformational change. That is, the helices of the HA trimer cannot maintain the closed form unless the C-terminal side of HA2 is embedded in the lipid membrane. Hence, calculation models in this work included the membrane mimicking the viral envelope and the transmembrane region of HA. TIP3P water molecules and ions to neutralize the calculation cell were generated to solvate the complex of HA and lipid membrane, making a